Applied Water Science (2023) 13:12
https://doi.org/10.1007/s13201-022-01821-1

ORIGINAL ARTICLE

# Using magnetite/zirconium-comodified attapulgite as a novel phosphorus (P) sorbent for the efficient removal of P and the adsorption mechanism allowing this effect

**Chengxun Deng[1] · Jianhui Xue[1,2,3] · Yongbo Wu[1,2]**

Received: 28 September 2022 / Accepted: 2 November 2022 / Published online: 21 November 2022


**Abstract**
Magnetite/zirconium-comodified attapulgite (Fe/ZrATP) acting as a novel phosphorus (P) sorbent was synthesized, characterized and applied to control P in an aquatic environment. Batch experiments demonstrated that at an adsorption dose of 0.2 g, 97.8% of the phosphate was rapidly sequestered from aqueous solution within 24 h, and the composite reached a maximal sorption capacity of 3 mg/g. The adsorption performance of the adsorbent Fe/ZrATP was minimally affected by changes in the initial pH (pH = 2–11). In addition, Fe/ZrATP presented excellent selectivity for phosphate when coexisting ions that often occur in water bodies were present; the solution ionic strength exerted little influence on phosphate sorption behavior. Adsorption and desorption experiments indicated that the removal of phosphate was mainly due to adsorption. The Fe/ZrATP adsorption isotherm was fitted to the Freundlich adsorption model. Moreover, the composite demonstrated excellent recyclability performance. The P adsorption mechanism of Fe/ZrATP involves electrostatic interactions, ligand exchange and surface precipitation. Our findings indicated that the separable Fe/ZrATP demonstrated high efficiency and sustainable phosphate removal, which is promising in phosphate removal and recovery applications

**Keywords** Magnetite/zirconium-comodified attapulgite · Phosphorus · Adsorption · Mechanism · Reusability

## Introduction

Excessive phosphorus (P) input leads to the eutrophication of freshwater bodies. Adsorption is widely used to remove a series of P-based pollutants from water because of its simple operation, good treatment effect and compatibility with reusable adsorbents (Rashid et al. 2021; Sun et al. 2011; Zhang et al. 2021). The development of materials for water purification and environmental remediation has attracted increasing attention from scholars (Liu et al. 2022; Qiu et al. 2022; Yao et al. 2022; Yu et al. 2021). Therefore, the development of efficient, safe and stable P adsorption passivation materials is the key to suppressing P release from freshwater bodies. In recent years, mineral-based P sorbents applied to control endogenous P release from sediments have received increasing attention from researchers (Kong et al. 2020; Reitzel et al. 2013; Spears et al. 2013). However, the recycling of adsorbent materials after their use in such applications has become a problem, as noted by many scholars (Ghosh and Bandyopadhyay 2016; Lin et al. 2020). If not properly handled, adsorbent materials will cause extensive harm to the environment. Moreover, the adsorption of P by many adsorbent materials is not satisfactory. Based on the above problems, there is an urgent need for a recyclable alternative with high adsorption capacity to control phosphate loading. Attapulgite (ATP) is widely available in nature, inexpensive and relatively unlikely to negatively impact aquatic environments (Ye et al. 2006). Moreover, due to its unique crystal structure, ATP has been applied in P adsorption techniques (Gan et al. 2009; Yin et al. 2017).

✉ Jianhui Xue
xjh1661832647@163.com

Chengxun Deng
478520742@qq.com

Yongbo Wu
yongbowu@njfu.edu.cn

[1] College of Biology and the Environment, Nanjing Forestry University, No. 159 Longpan Road, Nanjing 210037, China

[2] Co-Innovation Center for Sustainable Forestry in Southern China, Nanjing Forestry University, Nanjing 210037, China

[3] Institute of Botany, Jiangsu Province and Chinese Academy of Sciences, Nanjing 210014, China

ATP can load metal oxides, but few studies on this aspect have been reported worldwide. Preparing new modified ATP adsorbents to increase phosphate uptake is highly necessary. Lanthanum (La)-modified ATP and aluminum (Al)-modified ATP phosphate adsorbents have been explored to boost adsorption performance (Yin et al. 2020, 2022). However, Al compounds readily desorb $PO_4^{3-}$ under alkaline conditions (Egemose et al. 2010; Xu et al. 2017). Some studies have reported that chronic low-concentration accumulation of La in water bodies poisons aquatic organisms and humans (D'Haese et al. 2019). Interestingly, zirconium (Zr) species are environmentally friendly, nontoxic and chemically stable and have strong P affinity; zirconium-modified materials are considered very promising P adsorption passivation materials for active cover material applications (Chaudhry et al. 2017). Thus, Zr-based sorption materials have been investigated for phosphate removal techniques and have received increasing attention in recent years. Despite this information, only a few previous researchers have studied the recycling of Zr-modified adsorbents after their application. Adsorption materials are difficult to recycle, which limits their implementation in sustainable and large-scale applications.

In recent years, the use of magnetic adsorption materials to remove phosphate from aqueous solutions has attracted special attention in the field of water control because of its advantages, such as easy recovery from the environment and sustainable use (Bacelo et al. 2020; Jack et al. 2019; Kim et al. 2016). It has been reported that magnetite/lanthanum hydroxide composite exhibits significant magnetic and P adsorption capabilities, and they can be recovered through external magnetization fields (Lin et al. 2019; Song et al. 2020). The superiority of magnetic $Fe_3O_4$ nanomaterials over conventional adsorbent materials has been verified. It is necessary to consider the recyclability and reusability of P adsorption materials for eutrophic water remediation applications. Therefore, superparamagnetic $Fe_3O_4$ serves as a more ideal nanoparticle for the separation and reuse of ZrATP-based adsorption materials than sophisticated filtration and centrifugation options.

In this study, Fe/Zr-modified ATP (Fe/ZrATP) was prepared through chemical impregnation. Zr serves as the active sites for phosphate uptake in the adsorbent, and magnetic $Fe_3O_4$ is loaded on these sites to endow the adsorbent with separable and recoverable properties. The factors influencing the adsorption performance of Fe/ZrATP were investigated, as well as the adsorption kinetics of Fe/ZrATP. The recoverability properties were examined, and the mechanism associated with Fe/ZrATP adsorption of P was elucidated by diverse instrumental analyses.

## Materials and methods

### Materials

All the reagents in this study were of analytical grade, including NaCl, $NaNO_3$, $NaHCO_3$, $Na_2SO_4$, KCl, $MgCl_2$, $FeCl_3{\cdot}6H_2O$, $FeSO_4{\cdot}7H_2O$, NaOH, $ZrOCl_2{\cdot}8H_2O$ and $KH_2PO_4$. All the solutions in the experiment were prepared with deionized water unless otherwise specified. A series of phosphate solutions with concentrations ranging from 5 to 30 mg/L were prepared by dissolving different amounts of potassium dihydrogen phosphate in deionized water. The ATP used in the experiment was derived from Guangde County, Anhui Province. The solutions were buffered to pH levels of 10 with 0.1 mol/L NaOH.

### Preparation of magnetite/zirconium-comodified attapulgite (Fe/ZrATP)

Magnetite/zirconium-comodified attapulgite (Fe/ZrATP) was prepared by impregnation. The ATP was crushed and sieved through 100 mesh, and a 3% ATP suspension was made by adding deionized water. A 10% NaCl solution was mixed with the attapulgite suspension and stirred vigorously at 70 °C for 1 h. A solid sample was extracted by centrifuging the supernatant, and it was washed with water until no chloride ions (detected by 0.01 mol/L $AgNO_3$) were detected, at which point sodic attapulgite was obtained. Ten grams of ATP was weighed in a 1-L conical flask, 100 mL of $FeCl_3{\cdot}6H_2O$ solution and 100 mL of $FeSO_4{\cdot}7H_2O$ solution were added, and the pH was adjusted to 10with 1 mol/L NaOH solution. After stirring for 1 h with a constant-temperature magnetic stirrer at 344 r/min, 100 mL of $ZrOCl_2{\cdot}8H_2O$ was added, and the pH was slowly adjusted to 10.0 with NaOH solution. After standing for 12 h, the solid was centrifuged and washed repeatedly with deionized water 10 times, dried naturally and then ground through a 200 mesh sieve to obtain Fe/ZrATP.

### Batch adsorption experiments

#### Effects of adsorbent dosage on P adsorption

The adsorbent dosage gradient was 0.1, 0.2, 0.3, 0.5, 1.0, 1.5 and 2.0 (g); each dosage was mixed with 30 mL of 25-mg/L $KH_2PO_4$ (pH = 7) and shaken under the conditions of a temperature of 25 ℃ and a speed of 150 r/min for 24 h. The supernatant was filtered through a 0.45 μm membrane, 20 mL of the supernatant was extracted, the

supernatant was fixed with water to achieve a volume of 25 mL, and the absorbance was measured at 700 nm.

#### Effects of initial pH on P adsorption

20 mg/L of $KH_2PO_4$ solution was prepared with different pH values (pH = 2, 3, 4, 5, 6, 7, 8, 9, 10, 11). A total of 30 mL of each $KH_2PO_4$ solution with different pH values was extracted in a centrifuge tube. Then, 0.2 g of adsorbent material was added and mixed. The sample was shaken under a temperature of 25 °C and a speed of 150 r/min for 24 h, and 20 mL of the supernatant was extracted. Water was added to reach a volume of 25 mL. The absorbance was measured at a wavelength of 700 nm.

#### Effects of coexisting electrolytes on P adsorption

Solutions of NaCl, $NaNO_3$, $NaHCO_3$, $Na_2SO_4$, KCl and $MgCl_2$ (0.2 mol/L) were prepared, and 0.2 g of adsorbent material was weighed and added to 45 mL of 20 mg/L $KH_2PO_4$ solution (pH = 7, in terms of P) and 0.2 mol/L electrolyte mixture solution under a temperature of 25 °C and a speed of 150 r/min with shaking for 24 h. Afterward, 20 mL of supernatant was extracted. The absorbance was measured at a wavelength of 700 nm.

### Adsorption and desorption experiments

The absorbance was measured by weighing 0.2 g of adsorbent material, mixing it with 30 mL of 20 mg/L $KH_2PO_4$ solution (pH = 7, in terms of P) under a temperature of 25 °C and a speed of 150 r/min, shaking it for 24 h and then extracting 20 mL of supernatant (adsorption experiment). After adsorption, the adsorbent was mixed with 30 mL of 1 mol/L NaOH solution (desorption experiment), and 5 mL of the supernatant was extracted under a temperature of 25 °C and a speed of 150 r/min with shaking for 24 h. The absorbance was measured at a wavelength of 700 nm.

### Isothermal adsorption equilibrium thermodynamic experiments

$KH_2PO_4$ solutions (pH = 7, in terms of P) were prepared with different concentration gradients: 5, 10, 15, 20, 25 and 30 mg/L. 30 mL of $KH_2PO_4$ solutions of different concentrations were extracted in a 50 mL centrifuge tube; 0.2 g of absorbent material was added, the sample was shaken at 25 °C and 150 r/min, and then, the solids and liquids were separated. The supernatant was filtered through a 0.45-μm membrane, 20 mL of the supernatant was taken water was added and fixed until the sample reached a volume of 25 mL, and the absorbance was measured at a wavelength of 700 nm.

The equilibrium adsorption amount of the adsorbent material was calculated using the following equation:

$$q_e = \frac{(c_0 - c_e)v}{m} \quad (1)$$

where $q_e$ is the equilibrium adsorption amount (mg/g), $C_0$ and $Ce$ are the initial concentration and adsorption equilibrium concentration of P (mg/L), respectively, $V$ is the solution volume (L) and $m$ is the mass of the adsorbent used (g).

### Adsorption kinetics experiments

A total of 0.2 g of the adsorbent material was weighed in a 50-mL centrifuge tube, 25 mL of 20 mg/L $KH_2PO_4$ solution (as P, pH = 7) was added, and the sample was shaken at a temperature of 25 °C and a speed of 150 r/min for 48 h; 20 mL of the supernatant was extracted every 3 h, and water was added to reach a fixed volume of 25 mL. The absorbance was measured at a wavelength of 700 nm.

### Material characterization

The morphologies of the as-prepared materials were investigated with scanning electron microscopy (SEM) (SU8010, Japan Hitachi, Japan). We performed energy-dispersive spectroscopy (EDS) (Oxford Aztec, Oxford Instruments, UK) mapping of the materials to confirm the chemical constituents on the surface. An X-ray diffractometer (XRD) (TD-3500, Dandong Tongda, China) was used to observe the crystal phases of the materials. The functional groups and chemical bonds in the materials were determined with a Fourier transform infrared spectrometer (FTIR) (Nicolet iS 50 + Continuum Fourier, Thermo Fisher, USA). A gas-specific surface area pore size analyzer (based on the Brunauer–Emmett–Teller (BET) theory) (Tristar II3020, Macon Instruments, USA) was employed to detect the crystallographic phases. X-ray photoelectron spectroscopy (XPS) was performed with an X-ray photoelectron spectrometer (ESCAL AB250Xi, Thermo Scientific, USA) to analyze the element composition and valence state of the material surfaces.

## Results and discussion

### Characterization

Figure 1 shows scanning electron microscopy (SEM) images of attapulgite (ATP), Fe-modified attapulgite (FeATP), zirconium-modified attapulgite (ZrATP) and magnetite–zirconium-modified attapulgite (Fe/ZrATP). As shown in Fig. 1a, the ATP sample has a layer chain structure consisting of

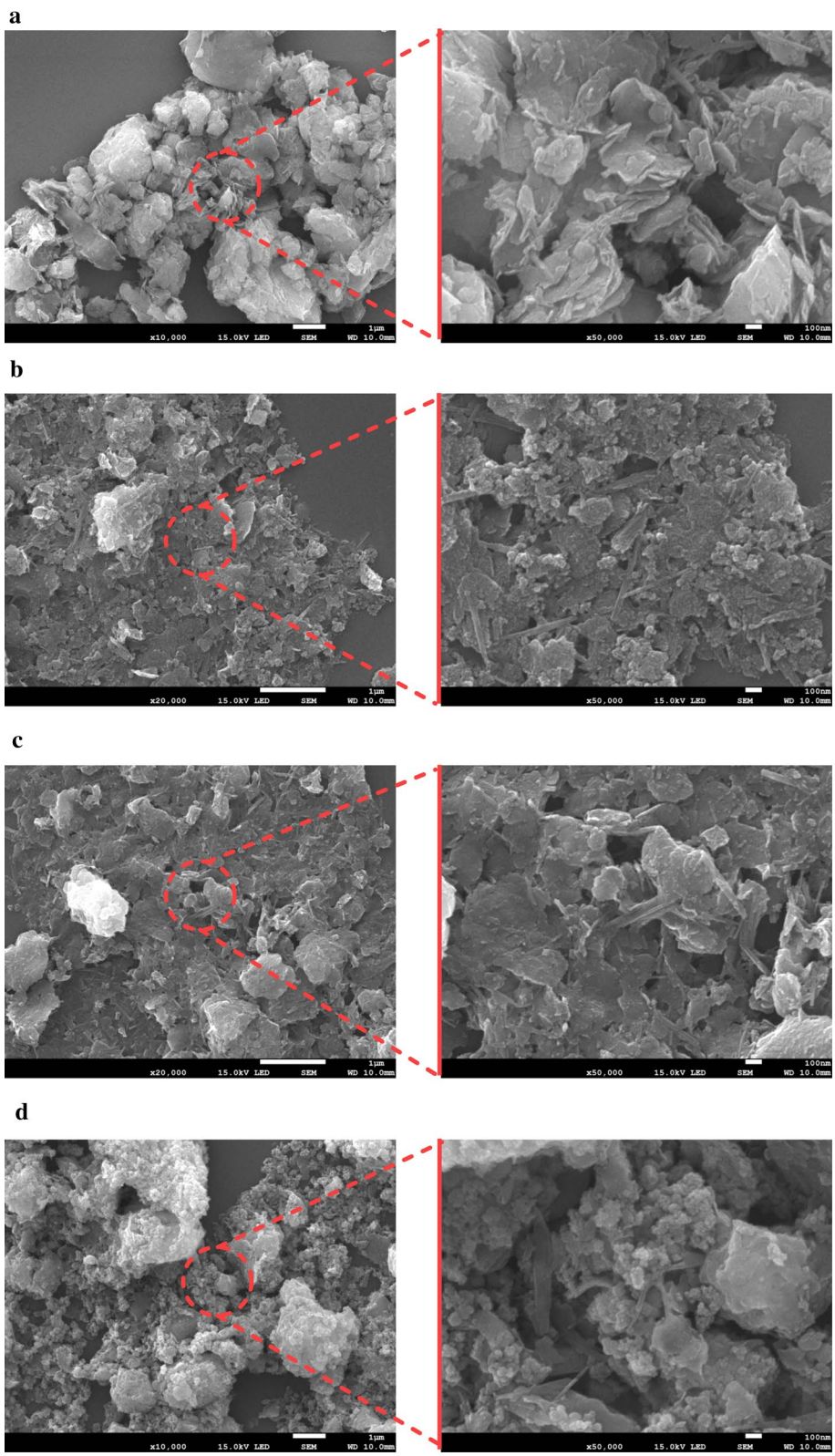


**Fig. 1** SEM images of ATP (**a**), FeATP (**b**), ZrATP (**c**) and Fe/ZrATP (**d**)

2:1 layered silicate units, each of which is connected to the next unit by a set of strong, Si–O–Si-bonded, inverted $SiO_4$ quadrangles, forming a unique pore structure and rod crystal morphology (McKeown et al. 2002). This phenomenon occurs because zeolite water and structured water accumulate on the surface of ATP as impurities (Manciu et al. 2007;

Zhou et al. 2020), obscuring the needlelike rod structure of the surface and appearing as an uneven lamellar structure in the SEM images, resulting in a small specific surface area. In FeATP synthesis, the structure of the water-loss part of the concave clay collapses after the high-temperature calcination of the iron-loaded concave clay. Due to the strong Fe–O force, the concave clay structure contracts and forms a pore-like lamellar structure with intercalated rod bundles in the lamellae (Fig. 1b). Fe is more uniformly dispersed on the surface of ATP. Relative to the ATP, the modified FeATP pore volume (0.14 cc/g) and the specific surface area (119.568 $m^2$/g) increase. Figure 1c shows granular zirconium oxide deposits on the adsorbent surface, indicating the successful preparation of the ZrATP adsorbent. Moreover, the ZrATP adsorbent structure is looser, and the pore channels increase; this phenomenon occurs mainly due to mixing of Zr between ATP layers during Zr loading of ATP, which increases its interlayer spacing. Fe/ZrATP exhibits a significantly improved morphology over those of ATP, FeATP and ZrATP, with increased surface roughness and fine voids and a significant increase in specific surface area (138.256 $m^2$/g) (Fig. 1d). Based on the overall surface morphology of the materials, ATP exhibits a relatively independent lamellar structure, while the modified FeATP, ZrATP and Fe/ZrATP all show aggregated small particles. In particular, the microstructure of Fe/ZrATP shows the characteristics of agglomerates, which indicates that the Fe/Zr metal compounds are combined well and loaded on the crystal surface of the raw material intaglio; the microstructure also indicates that the surface morphology of the synthesized material is significantly changed and that the formation of agglomerate structure increases the significance of the phosphate chemisorption.

The energy-dispersive spectroscopy (EDS) characterization results of the ATP, FeATP, ZrATP and Fe/ZrATP samples are shown in Fig. 2. The surface element mass percentages on ATP descend in the order Si, O, C, Zr, Fe, Al, Mg, Ca and K (Fig. 2a). The surface element mass percentages on FeATP descend in the order Si, O, Zr, Fe, Na, Al and Mg (Fig. 2b). The surface element mass percentages on ZrATP descend in the order Si, O, C, Zr Al, Fe, Mg, Na, Ca and K (Fig. 2c). The Fe/ZrATP surface element mass percentages descend in the order Si, O, C, Zr, Fe, Ca, Na, Mg, Al and K (Fig. 2d). According to the compositions of the materials, the main elements of all four materials are Si, O and C, which are the main constituent elements of the raw material concave attapulgite. However, there are differences between the mass percentages of Si. The mass percentages of Si in the ATP, FeATP, ZrATP and Fe/ZrATP samples are 63.9%, 78.8%, 60.2% and 34.4%, respectively. The percentage of the metal element Zr in ZrATP is higher than that of ATP, and the analyses confirm that a certain amount of Zr is present on the outer surfaces of the composite, indicating that Zr has been successfully loaded on ZrATP. The contents of Zr and Fe in ATP after Fe/Zr modification are much greater than those of the raw material, and the metal elements are primarily Fe/Zr. The above results indicate that the metallic elements Fe and Zr have been successfully loaded onto the surface of ATP.

An automatic specific surface and porosity analyzer is used to obtain the physical property parameters, such as the specific surface area, pore volume and pore size distribution. The specific surface area of Fe/ZrATP (138.256 $m^2$/g) is obviously greater than that of ATP (100.37 $m^2$/g), which may be because the metal elements Fe and Zr are not only distributed on the surface of ATP but also enter the pores of the concavite in small amounts, increasing the layer spacing of the material and forming a bilayer structure with an increased surface area (Nguyen et al. 2022). Then, the specific surface area of Fe/ZrATP increases again due to the uniform load of $Fe_3O_4$, which yields a rough composite surface, as observed from the SEM images in Fig. 1d. The data in Table 1 show that the pore diameter and volume of Fe/ZrATP are 0.101 cc/g and 3.396 nm, respectively, indicating that Fe/ZrATP possesses a relatively large surface area, which is a prerequisite for sorbents to exhibit good sorption performance (Wei et al. 2022).

To investigate the crystal structures of the materials, X-ray diffraction (XRD) was performed, and the obtained XRD patterns are presented in Fig. 3. Moderate ATP diffraction is typically detected at $2\theta = 19.9°$, 30.9° and 40.4°, and the strong diffraction at 26.6° represents quartz in the (011) plane, which is in agreement with previous research findings (Allawi et al. 2022). The diffraction peak of ATP at 26.9° is a characteristic peak of quartz, indicating that ATP contains a certain amount of quartz sand (Kong et al. 2021). After Fe and Zr modification, a sharp strong peak at 35.4° for the (311) plane is clearly observed (Fang et al. 2017), corresponding to the characteristic peak of $Fe_3O_4$ diffraction, which indicates the successful surface coating of magnetic $Fe_3O_4$ on attapulgite. Similarly, the characteristic peak of $ZrO_2$ appears at 30.2° for the (111) plane, which demonstrates that Zr is effectively loaded on Fe/ZrATP in the form of $ZrO_2$ (Ohashi et al. 2022). In addition, the FeATP, ZrATP and Fe/ZrATP materials all show different degrees of weakening of the peak intensity at the characteristic peaks compared to that of ATP. This phenomenon may occur because the metal elements Fe and Zr are not only distributed on the surface of the ATP but also enter the pores of the concavite in small amounts, increasing the layer spacing of the material and forming a bilayer structure with an increased surface area. This finding corresponds to the surface morphology shown by the SEM images and the physical property parameters (specific surface area, pore volume and pore size distribution) of the modified ATP, indicating the successful synthesis of FeATP, ZrATP and Fe/ZrATP.

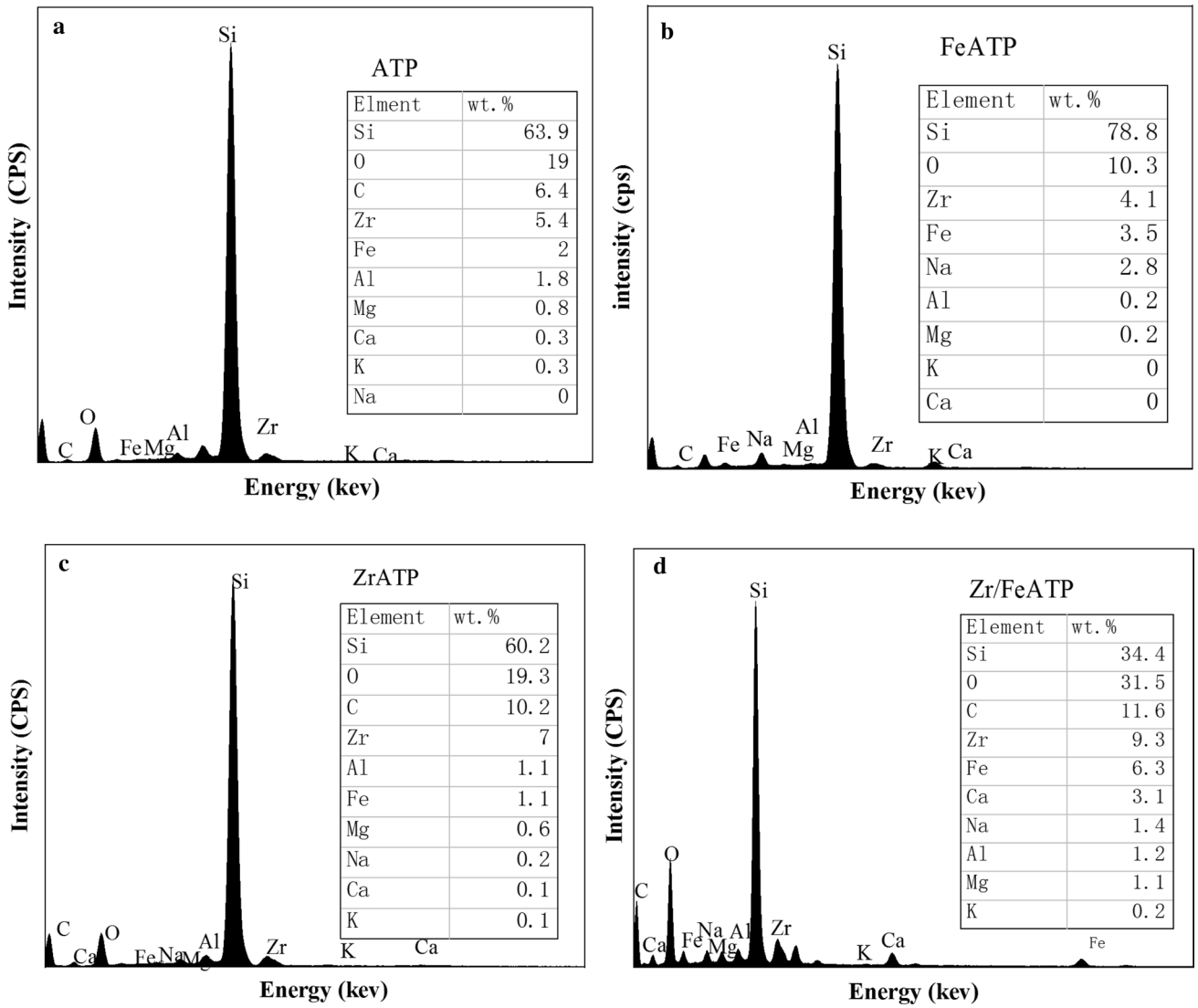


**Fig. 2** EDS results of ATP (**a**), FeATP (**b**), ZrATP (**c**) and Fe/ZrATP (**d**)

**Table 1** BET properties of ATP, FeATP, ZrATP and Fe/ZrATP

| Sample | ATP | FeATP | ZrATP | Fe/ZrATP |
|---|---|---|---|---|
| BET surface area ($m^2$/g) | 100.37 | 119.568 | 102.919 | 138.256 |
| Pore diameter (nm) | 3.427 | 3.048 | 3.42 | 3.396 |
| Pore volume (cc/g) | 0.14 | 0.136 | 0.157 | 0.101 |

For the qualitative analysis of functional groups, Fourier transform infrared spectroscopy (FTIR) was performed, and the obtained FTIR spectra of ATP, FeATP, ZrATP and Fe/ZrATP are shown in Fig. 4. The peaks near 3620–3397 $cm^{-1}$ are attributed to the symmetric and asymmetric stretching modes of molecular water coordinated to the magnesium (or alternative cation for ATP) at the edges of the channels and the bending vibration of the hydroxide radical (OH)

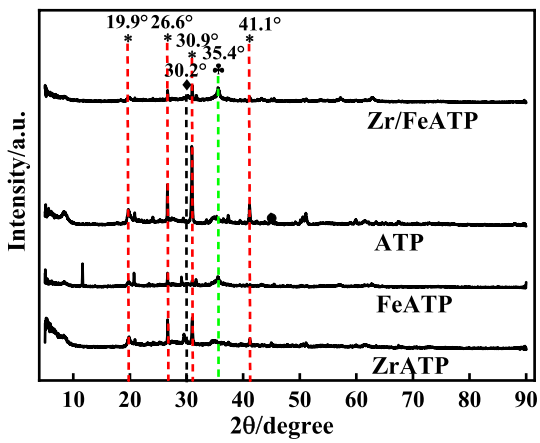


**Fig. 3** XRD patterns of ATP (**a**), FeATP (**b**), ZrATP (**c**) and Fe/ZrATP (**d**) (*: ATP, ◆: ZrO2, ♣: $Fe_3O_4$)

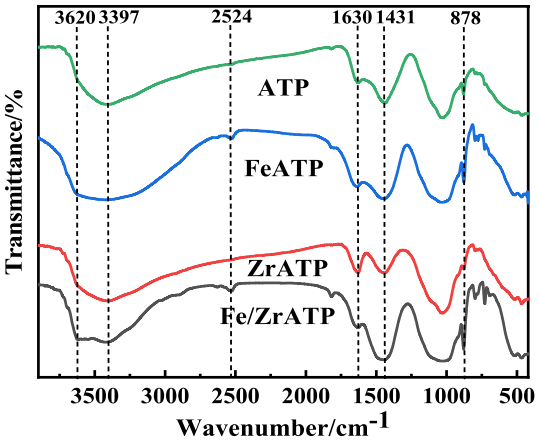


**Fig. 4** FTIR spectra of ATP, FeATP, ZrATP and Fe/ZrATP

bond of chemisorbed water, respectively (Pan et al. 2010). In addition, characteristic peaks are present at 1630 $cm^{-1}$ and 1431 $cm^{-1}$ for all four materials, attributed to the bending vibration of Mg–O and the stretching vibration of Si–O–Al bonds, respectively, which are typical of ATP (Hekimoğlu and San 2022). The band at 878 $cm^{-1}$ is due to the bending vibration of Si–O–Si bonds. Compared with ATP and FeATP, the characteristic peaks at 878 $cm^{-1}$ in the composite ZrATP and Fe/ZrATP composite show a redshift, indicating that Zr has been successfully embedded in ATP (Frost et al. 2010). Compared to ATP and ZrATP, FeATP and Fe/ZrATP show a new peak at 2524 $cm^{-1}$, which is designated as Fe–O vibrations in $Fe_3O_4$, indicating the presence of particles of $Fe_3O_4$ in the composite (Nkinahamira et al. 2020). From the above analysis, it can be concluded that Fe/ZrATP was successfully synthesized.

## Batch sorption experiments

### Effects of adsorbent dosage on P adsorption

The effect of adsorbent dosage on the removal efficiency and adsorption capacity of phosphate by the adsorbents is shown in Fig. 5a and b. The phosphate removal efficiency was 85.3% with the addition of 0.1 g FeATP and 97.8% with 0.3 g FeATP, after which point the removal efficiency remained almost unchanged with the continued addition of FeATP. This observation indicates that Fe-modified ATP displayed a stronger phosphate adsorption ability because

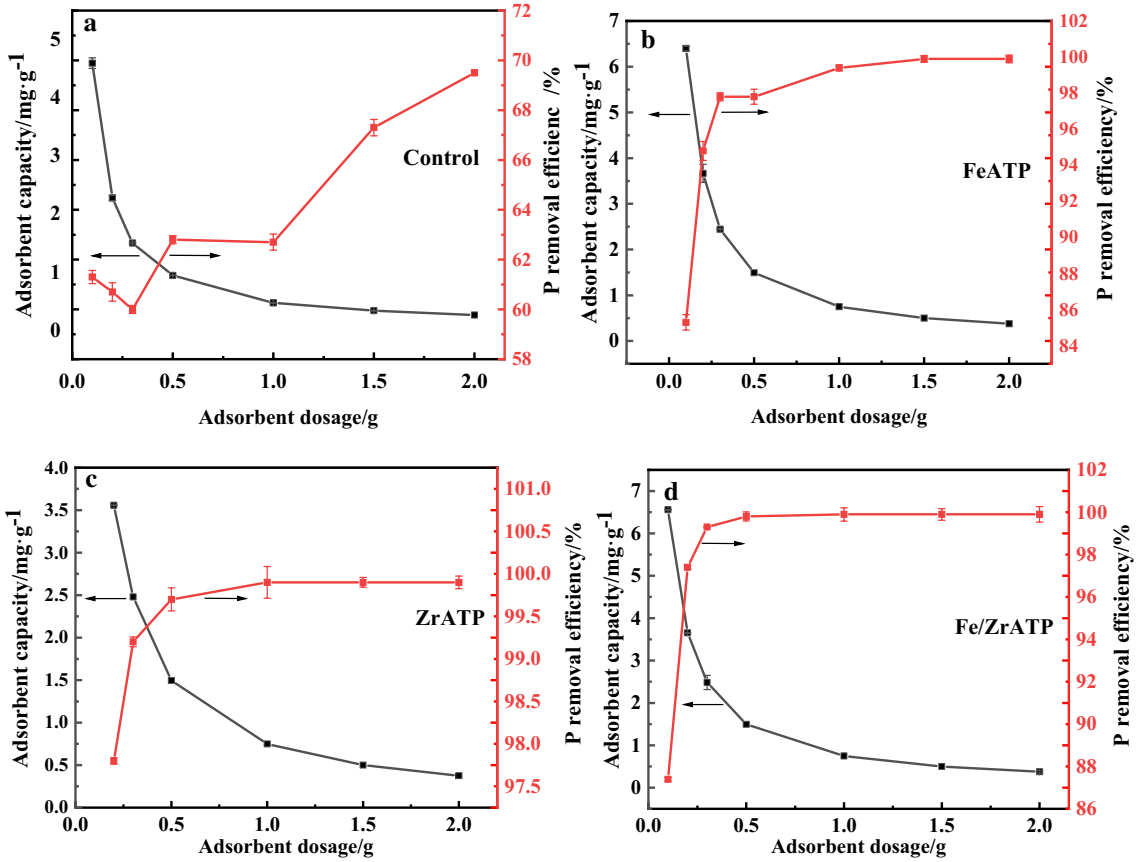


**Fig. 5** Effects of adsorbent dosage on P adsorption for ATP (**a**), FeATP (**b**) and ZrATP (**c**), Fe/ZrATP (**d**)

Fe was more uniformly dispersed on the surface of ATP (Zhu et al. 2022). Moreover, the pore size of the modified FeATP was contracted relative to that of ATP, and the specific surface area increased, resulting in a larger contact surface with phosphate. As shown in Fig. 5c and d, with the increase in the mass of the adsorbent from 0.1 to 2 g, the phosphate removal efficiency of ZrATP and Fe/ZrATP showed a trend of first increasing and then stabilizing before the adsorption capacity gradually decreased. The removal efficiency reached 99.7% and 99.8% when 0.3 g of the adsorbents ZrATP and Fe/ZrATP was added, respectively. The combination of Zr with ATP causes the material structure to be loose, the pores to become larger and the specific surface area to increase. However, with an increase in adsorbent dosage, the adsorption capacity of the four materials continued to decrease, and the removal of phosphate in the system gradually stabilized after the initial increase. The above results indicated that increasing the dosage of materials could increase the effective adsorption sites and thus improve the phosphate adsorption performance. In addition, the addition of iron made the material magnetic for recovery, so Fe/ZrATP was shown to be the best material to adsorb the P released from the substrate.

### Effects of initial pH on P adsorption

The effects of pH on the phosphate sorption of ATP, FeATP, ZrATP and Fe/ZrATP were studied under pH values ranging from 2 to 11, and the results are shown in Fig. 6. Compared with other adsorbents, Fe/ZrATP has a high phosphate adsorption capacity in the pH range of 2–11 and a relatively stable adsorption capacity. The adsorption amount of P showed a trend of slowly decreasing with increasing pH, indicating that the adsorbent Fe/ZrATP had a better adsorption effect on phosphate and was less affected by acid and alkali (Zhang et al. 2016). The reason for the slow decreasing trend is the deprotonation of Fe/ZrATP, which leads to electrostatic repulsion between Fe/ZrATP and phosphate. In addition, an increase in pH leads to an increase in $OH^-$ concentration in the environment, which will inhibit the hydrolysis of metal oxides on the surface of the modified material and hinder the binding process of phosphate and metal ions. Additionally, the high concentration of $OH^-$ will compete with phosphate ions on the adsorbent material, resulting in poor phosphorus removal performance. With increasing pH, electrostatic repulsion between Fe/ZrATP and phosphate occurs due to the deprotonation of the composite. The increase in the pH level leads to an increase in the $OH^-$ concentration in the environment, which inhibits the hydrolysis of the metal oxides on the surface of the modified material and hinders the binding process between the phosphate and metal ions; the high $OH^-$ concentration competes with phosphate ions for adsorption on the material, leading to poor phosphorus removal performance. Moreover, Fig. 6 obviously shows that the phosphate adsorption performance of FeATP was extremely unstable due to the influence of pH, probably due to the inability of some phosphate ions to bind to the adsorption sites on the FeATP surface under neutral FeATP conditions. The above results indicated that the pH stability of the Fe/ZrATP composite was still much higher than those of many other Zr-based adsorbents, as previously reported.

### Effects of coexisting electrolytes on P adsorption

The aim of this experiment was to investigate the effects of $Na^+$, $K^+$, $Mg^{2+}$, $Ca^{2+}$, $Cl^-$, $SO_4^{2-}$ and $HCO_3^{2-}$, anions often found in water bodies, on the phosphate removal performance of ATP, FeATP, ZrATP and Fe/ZrATP. Figure 7 shows that the effects of coexisting electrolytes on P

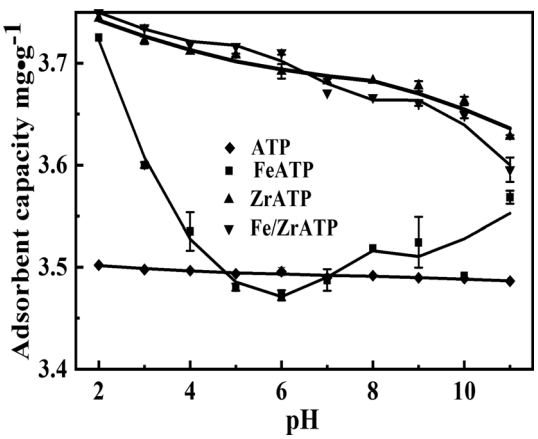


**Fig. 6** Effects of initial pH on P adsorption

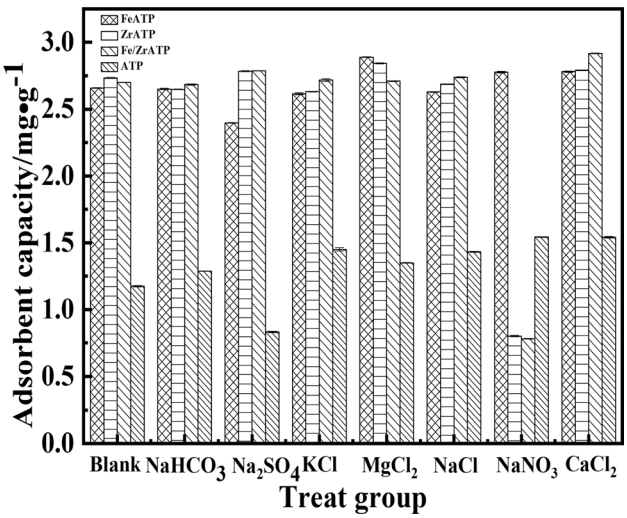


**Fig. 7** Effects of coexisting electrolytes on P adsorption

adsorption were not obvious and could be nearly ignored (< 1%) when the adsorption capacities of FeATP, ZrATP and Fe/ZrATP were all above 2.7 mg/g. Overall, when anions and phosphates coexisted, the modified adsorbents FeATP, ZrATP and Fe/ZrATP all adsorbed higher amounts of phosphate than ATP, with Fe/ZrATP adsorbing the most on average. This adsorption phenomenon demonstrated that the composite had high sorption selectivity for phosphate, which is consistent with the results of the previous study on the effects of other factors on phosphate adsorption performance.

## Behaviors and mechanisms of phosphate adsorption by the adsorbent Fe/ZrATP

### Adsorption and desorption experiments

To obtain insight into the sorption behavior and mechanism of phosphate by the adsorbent Fe/ZrATP, a series of adsorption and desorption experiments were performed (Fig. 8). The results of desorption of the adsorbed saturated material using 1 mol/L NaOH show that the adsorption capacity of Fe/ZrATP can still reach the level of the original adsorbent. The above results indicate that the NaOH desorption method is applicable to Fe/ZrATP. Desorption with a higher concentration of NaOH solution mainly occurs due to the strong ligand exchange processes of $H_2PO_4^-$, $HPO_4^{2-}$ and hydroxyl groups on the surface of ATP, which allows the adsorbed phosphate to be desorbed from the material. This result may be due to the $OH^-$ in the system promoting the adsorption of $Zr^{4+}$ and $Fe^{2+}$ in the raw material to form phosphorite precipitates from the $HPO_4^{2-}$ in water. NaOH solution at 1 mol/L shows very high desorption of Fe/ZrATP, which illustrates that the removal of phosphate by the adsorbent Fe/ZrATP is mainly achieved through the ligand exchange process.

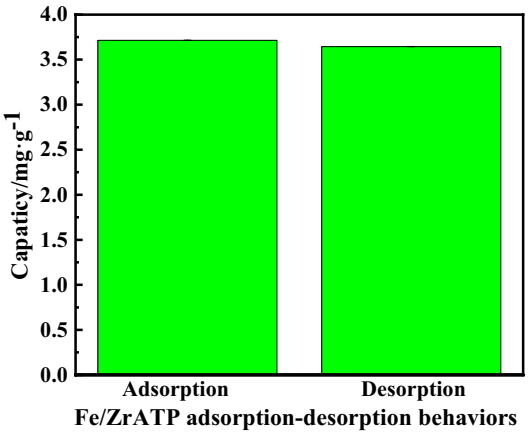


**Fig. 8** Effect of initial phosphate concentration on phosphate sorption performance by the adsorbent Fe/ZrATP

### Adsorption isotherm

Adsorption isotherms can describe the correlation between the adsorbent and adsorbate, which is important for further revealing the adsorption mechanism. The common adsorption isotherm models are the Freundlich and Langmuir adsorption models. The simulation parameters related to the isothermal adsorption of Fe/ZrATP were derived by fitting the adsorption experimental data with the Freundlich and Langmuir adsorption models, which are listed in Table 2. The correlation coefficients $R^2$ are close to 1, but according to the adsorption conditions, the surface of Fe/ZrATP is inhomogeneous and does not satisfy the assumptions of the Langmuir adsorption isotherm model. Therefore, the phosphate adsorption performance of Fe/ZrATP satisfies the Freundlich model. By comparing the Freundlich model parameters of ATP, ZrATP, FeATP and Fe/ZrATP, we find that Fe/ZrATP exhibits the best combined adsorption performance.

### Adsorption kinetics of Fe/ZrATP

The kinetic fitting models of Fe/ZrATP for phosphate sorption are shown in Fig. 9a. The Fe/ZrATP adsorption parameters were fitted by pseudo-first-order and pseudo-second-order kinetic models, and the two models achieved similar sorption capacities despite differences in their respective rate constants (resulting from model equation variations). The results indicated that the experimental adsorption data of Fe/ZrATP were better fitted by the pseudo-second-order model ($R^2 = 0.966$) (Table 3). Moreover, the theoretical adsorption capacity ($q_e$) calculated by this model was closer to

**Table 2** Isothermal adsorption simulation parameters of ATP, ZrATP, FeATP and Fe/ZrATP

| Isotherm model | Parameter | ATP | FeATP | ZrATP | Fe/ZrATP |
|---|---|---|---|---|---|
| Freundlich isotherm model $q = k\rho^{1/n}$ | $k$ (mg/$^{(1-1/n)}$L$^{1/n}$/g) | 0.035 | 0.156 | 0.153 | 0.155 |
| | $1/n$ | 1.304 | 0.975 | 0.985 | 0.983 |
| | $R^2$ | 0.998 | 1.000 | 0.999 | 1.000 |
| Langmuir isotherm model $q = \frac{k \cdot q_m \cdot \rho}{1+k \cdot \rho}$ | $q_m$ (mg/g) | / | 86.96 | 166.7 | 166.7 |
| | $k$ (L/mg) | / | 0.0017 | 0.0009 | 0.0009 |
| | $R^2$ | 0.999 | 1.000 | 1.000 | 1.000 |

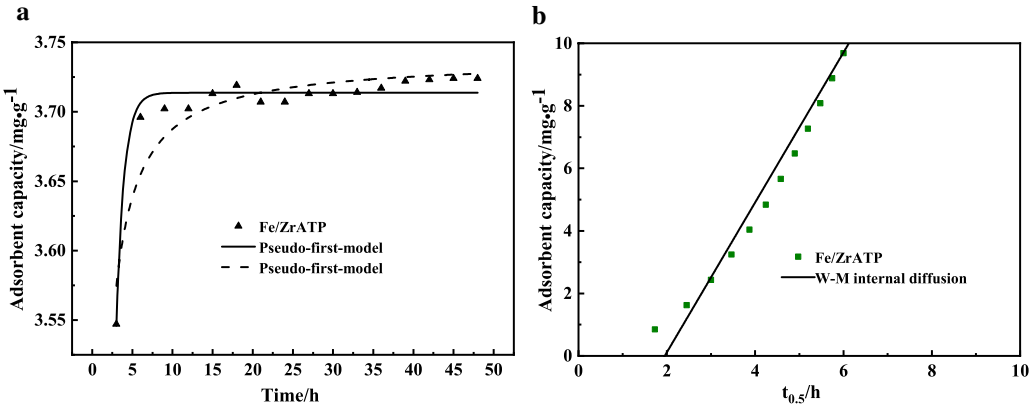


**Fig. 9** Kinetic models (**a**) and W–M internal diffusion model (**b**) of Fe/ZrATP

the experimental value, further confirming that the pseudo-first-order kinetic model was better and that chemisorption dominated the adsorption process (Guo et al. 2020). In the initial stages of adsorption, the adsorption amount increased rapidly because the abundant adsorption sites on the surface of Fe/ZrATP were adsorbed with phosphate. At this point, phosphate adsorption was accomplished by surface adsorption or rapid boundary layer diffusion on the outer surface. Then, the phosphate molecules diffused into the internal porous structure of ATP, which was in the internal diffusion stage. After a period of time, the adsorption sites on the surface of ATP gradually decreased, and the concentration of phosphate in the solution gradually decreased, leading to a slow increase in the adsorption capacity and reaching the saturation equilibrium adsorption amount after 48 h. At this stage, the adsorption system was in the dynamic equilibrium of the adsorption–desorption process. The Weber–Morris (W–M) internal diffusion model was used to fit the experimental data; Fe/ZrATP showed substantially different results of W–M kinetic equation fitting (Fig. 9b). The W–M equation is mainly used to determine whether the internal diffusion of the adsorbate into the adsorbent material particles is the controlling step of the adsorption process. The fitted equation of Fe/ZrATP was very close to a straight line passing through the origin with a fitted $R^2$ value of 0.972 (Table 3), indicating a relatively good linear correlation. In addition, the above results illustrated that the mass transfer rate in the internal diffusion stage played a role in the adsorption of phosphate by Fe/ZrATP.

**Table 3** Fitting parameters of the pseudo-first-order kinetic, pseudo-second-order kinetic and internal diffusion models for Fe/ZrATP adsorption

| Kinetic model | Parameter | Fe/ZrATP |
|---|---|---|
| Pseudo-first-order model | $q_{e,exp}$ (mg/g) | 3.724 |
| $q_t = q_e\left(1 - \exp\left(-k_1 t\right)\right)$ | $q_{e,cal}$ (mg/g) | 3.714 |
| | $k_1$ (1/min) | 1.033 |
| | $R^2$ | 0.966 |
| Pseudo-second-order model | $q_{e,exp}$ (mg/g) | 3.724 |
| $q_t = \frac{k_2 q_e^2 t}{1+k_2 q_e t}$ | $q_{e,cal}$ (mg/g) | 3.738 |
| | $k_2$ (g/(mg·min)) | 1.951 |
| | $R^2$ | 0.861 |
| W–M internal diffusion | $k_{i,d}$ (mg/(g·min$^{0.5}$)) | 2.399 |
| $q_t = k_{i,d} t^{0.5} + c$ | $C$ (mg/g) | − 4.685 |
| | $R^2$ | 0.972 |

## Mechanism of chemical adsorption

The above adsorption behaviors, adsorption isotherms and adsorption kinetics indicate that the dominant adsorption mechanism of Fe/ZrATP is ligand exchange (Awual et al. 2014; Huang et al. 2016). Initially, the Fe/ZrATP surface hydroxyl groups are usually covered by phosphate solution, after which Fe/ZrATP starts to capture phosphate by a process of ligand exchange, in which the hydroxyl groups on the Fe/ZrATP surface are replaced by phosphate, forming covalent bonds between the ligand and metal atoms (Bai et al. 2016; Kong et al. 2021). According to the SEM and BET correlation analyses, the Fe/ZrATP surface exhibits increased roughness, fine voids and a significant increase in the specific surface area. Therefore, Fe/ZrATP, as a selective ligand exchanger, can readily adsorb phosphate even if the ligand concentration in solution is low. The active ligand exchange between the hydroxyl group on the surface of ATP and $PO_4^{3-}$ in water is an important mechanism for phosphate adsorption, and the −OH on the metal binding site on the surface of the material can exchange ligands with the negatively charged phosphate, effectively increasing the phosphate adsorption amount (Eq. (2)). In addition, the adsorption of phosphate in water by modified ATP is not a single chemical interaction but involves a cross-coupling of

several interactions that govern the adsorption behavior under certain conditions. In this study, two other chemical interactions cannot be neglected: electrostatic interaction and surface precipitation. The pH of the solution system plays an important role in the electrostatic interaction during adsorption of adsorbents; therefore, Fe/ZrATP with a more positive charge can better adsorb phosphate (Yang et al. 2020). However, the electrostatic effect may be weakened by the solvent effect in the solution system, ion masking and other factors (Eq. (3)). Surface precipitation plays a role in the adsorption of phosphate. The metal ions ($Zr^{4+}$, $Fe^{2+}$) on the surface of Fe/ZrATP form deposits or stable inorganic substances with the surface of phosphate in water. Increasing the content of Zr/Fe leads to an increase in the amount of precipitation and further enhances the adsorption efficiency (Eqs. (4) and (5)). Therefore, ligand exchange plays a dominant role in phosphate adsorption by Fe/ZrATP, accompanied by electrostatic interactions and surface precipitation during the adsorption process. The adsorption mechanism of Fe/ZrATP for phosphate adsorption is shown in Fig. 10.

$$\mathrm{Fe/Zr-OH} + \mathrm{H_2PO_4^-} \rightarrow \mathrm{Fe/Zr-H_2PO_4} + \mathrm{OH^-} \quad (2)$$

$$(\mathrm{Fe/Zr})^{n+} + \mathrm{PO_4^{3-}} \rightarrow (\mathrm{Fe/Zr})_3(\mathrm{PO_4})_n \quad (3)$$

$$\mathrm{Zr^4} + 2\mathrm{HPO_4^{2-}} + \mathrm{H_2O} \rightarrow \mathrm{Zr(HPO_4)_2 \cdot H_2O} \downarrow \quad (4)$$

$$\mathrm{Fe^{2+}} + \mathrm{HPO_4^{2-}} + \mathrm{H_2O} \rightarrow \mathrm{FeHPO_4 \cdot H_2O} \downarrow \quad (5)$$

## XPS analysis of Fe/ZrATP after P absorption

The previous chemical composition and chemical state of Fe/ZrATP were further explored after phosphate adsorption studies for the surface complexation of phosphate with Fe/ZrATP using X-ray photoelectron spectroscopy (XPS). The XPS measurements and high-resolution spectra are shown in Fig. 11. The full XPS spectra indicated the presence of several elements, including oxygen (O), carbon (C), calcium (Ca), Fe and Zr, on the surface of Fe/ZrATP (Fig. 11a). After phosphate adsorption using Fe/ZrATP, the three binding energies of P 2p (133.48, 132.94 and 132.68 eV) were located between 132.3 and 135.2 eV, which was attributed to electrostatic gravitational interactions of the metal ions on the Fe/ZrATP surface with $HPO_4^{2-}$ and $H_2PO_4^-$ (Fig. 11b). The results show that $HPO_4^{2-}$ and $H_2PO_4^-$ coexist on the surface of Fe–/ZrATP, forming Fe–P and Zr–P precipitates. After adsorption of phosphate by Fe/ZrATP, the binding energy of Fe 2p slightly increased, indicating possible electron transfer in the Fe 2p valence band and the formation of Fe–O–P inner-sphere coordination (Fig. 11c and d). Zr 3d absorption peaks were observed at 183.98 eV and 181.68 eV before phosphate adsorption by Fe/ZrATP Fig. (11e). The representative satellite peaks of Zr 3d for Fe/ZrATP after phosphate adsorption are centered at 184.08 eV and 181.78 eV (Fig. 11f). This result may be due to the binding of P–Zr–O, which subsequently led to the formation of Zr–O–P inner-sphere coordination (Fig. 11f). The results of XPS analysis further verified the mechanism analysis results, and the two conclusions were consistent, indicating that the adsorption removal of phosphate by Fe/ZrATP is achieved by the combined effect of ligand exchange, electrostatic interactions and surface precipitation.

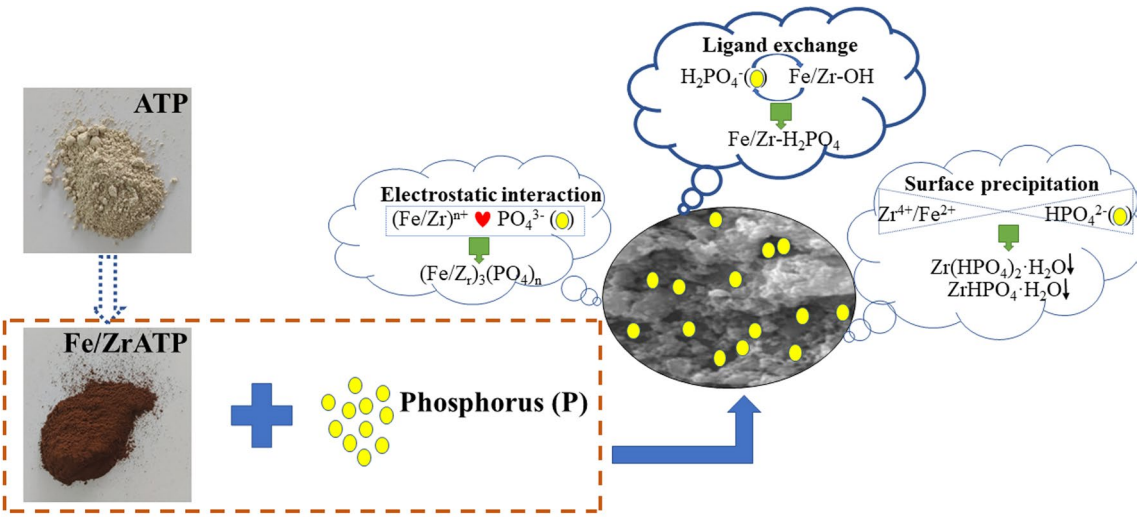


**Fig. 10** Mechanism of phosphate removal by the Fe/ZrATP composite

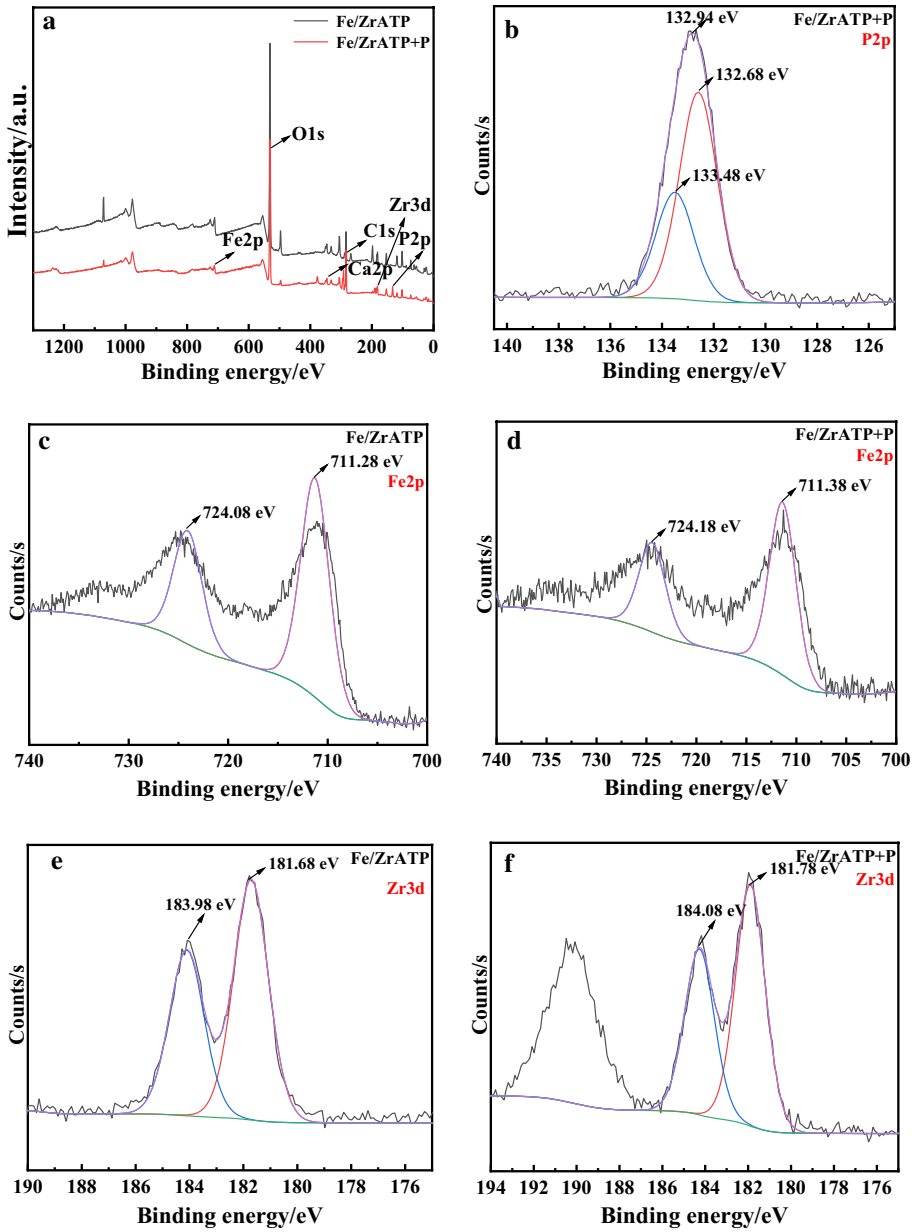


**Fig. 11** High-resolution XPS spectra: survey (**a**), P 2p (**b**), Fe 2p (**c** and **d**) and Zr 3d spectra (**e** and **f**) for Fe/ZrATP before and after phosphate absorption

## Conclusion

In this study, magnetically recyclable Fe/Zr-comodified ATP (Fe/ZrATP) composite were developed through a chemical impregnation method to achieve economical, highly efficient and selective P removal from water. The results of this study indicated that the P removal efficiency of Fe/ZrATP was greatly enhanced and reached 97.8%. The newly prepared sorbent (Fe/ZrATP) performed well at pH levels ranging from 2 to 11 and exhibited specific selectivity toward ionic phosphate. Batch adsorption experiments revealed that Fe/ZrATP displayed excellent adsorption performance for phosphate. The isotherm and kinetic experimental data for Fe/ZrATP were fitted well by the Freundlich isotherm model ($R^2 = 1$) and the pseudo-first-order model ($R^2 = 0.972$). The adsorption mechanism analysis and XPS results together verified that Fe/ZrATP achieves phosphate removal under the combined effect of ligand exchange, electrostatic interactions and surface precipitation. Moreover, Fe/ZrATP could be successfully recovered by magnetism. The novelty of this study lies in the use of cost-controllable and simple technology to produce adsorption materials with a high adsorption capacity and wide pH range. In conclusion, Fe/ZrATP could be used as a highly efficient and remarkable phosphate removal adsorbent material to solve P pollution problems in water.

**Author contributions** CD was responsible for methodology, investigation, visualization and writing the original draft. JX was involved in methodology, investigation, funding acquisition and writing, reviewing and editing. YW took part in conceptualization, methodology, investigation, visualization, supervision, resources and funding acquisition.

**Funding** This research was supported by Major State Basic Research Development Program of China, Grant No. 2016YFC0502605, and the National Science and Technology Program during the Twelfth Five-Year Plan Period, Grant No. 2015BAD07B0404, Jianhui Xue.

## Declarations

**Conflict of interest** The authors declare that there are no conflicts of interest in this study.



## References

Allawi AH, Mohammed MY, Ayrim NB, Alheety MA, Mahmood AR (2022) Synthesis of attapulgite-MnO2 nanocomposite from manganese complex by ultrasound for hydrogen storage. J Indian Chem Soc 99(8):100596

Awual MR, Shenashen MA, Jyo A, Shiwaku H, Yaita T (2014) Preparing of novel fibrous ligand exchange adsorbent for rapid column-mode trace phosphate removal from water. J Ind Eng Chem 20(5):2840–2847

Bacelo H, Pintor AMA, Santos SCR, Boaventura RAR, Botelho CMS (2020) Performance and prospects of different adsorbents for phosphorus uptake and recovery from water. Chem Eng J 381:122566

Bai Y, Dou YB, Xie LH, Rutledge W, Li JR, Zhou HC (2016) Zr-based metal–organic frameworks: design, synthesis, structure, and applications. Chem Soc Rev 45(8):2327–2367

Chaudhry SA, Zaidi Z, Siddiqui SI (2017) Isotherm, kinetic and thermodynamics of arsenic adsorption onto Iron-Zirconium Binary Oxide-Coated Sand (IZBOCS): modelling and process optimization. J Mol Liq 229:230–240

D'Haese Patrick C, Douglas Grant, Verhulst Anja, Neven Ellen, Behets Geert J, Vervaet Benjamin A, Finsterle Karin, Lürling Miquel, Spears Bryan (2019) Human health risk associated with the management of phosphorus in freshwaters using lanthanum and aluminium. Chemosphere 220:286–299

Egemose S, Reitzel K, Andersen FØ, Flindt MR (2010) Chemical lake restoration products: sediment stability and phosphorus dynamics. Environ Sci Technol 44:985–991

Fang L, Wu B, Lo IMC (2017) Fabrication of silica-free superparamagnetic $ZrO_2$@$Fe_3O_4$ with enhanced phosphate recovery from sewage: performance and adsorption mechanism. Chem Eng J 319:258–267

Frost RL, Xi YF, He HP (2010) Synthesis, characterization of palygorskite supported zero-valent iron and its application for methylene blue adsorption. J Colloid Interface Sci 341:153–161

Gan F, Zhou J, Wang H, Du C, Chen X (2009) Removal of phosphate from aqueous solution by thermally treated natural palygorskite. Water Res 43:2907–2915

Ghosh SK, Bandyopadhyay A (2016) Characterizing acidic fly ash with and without biomass combustion residue for adsorptive removal of crystal violet with optimization of mixed adsorbent by response surface modeling. Earth Sci Environ. https://doi.org/10.1007/s12665-016-5571-z

Guo CB, Zou JJ, Yang JL, Wang KH, Song SY (2020) Surface characterization of maize-straw-derived biochar and their sorption mechanism for $Pb^{2+}$ and methylene blue. PLoS ONE 15(8):e0238105

Hekimoğlu G, Sarı A (2022) Shape stabilized attapulgite/myristic-palmitic acid composite PCM for thermal energy storage implementations in buildings. Mater Today: Proc 58:1350–1353

Huang LJ, He M, Chen B, Hu BB (2016) A mercapto functionalized magnetic Zr-MOF by solvent-assisted ligand exchange for $Hg^{2+}$ removal from water. J Mater Chem A 4(14):5159–5166

Jack J, Huggins TM, Huang Y, Fang Y, Ren ZJ (2019) Production of magnetic biochar from waste-derived fungal biomass for phosphorus removal and recovery. J Clean Prod 224:100–106

Kim YH, Sim B, Choi HJ (2016) Fabrication of magnetite-coated attapulgite magnetic composite nanoparticles and their magnetorheology. Colloids Surf A Physicochem Eng Asp 507:103–109

Kong L, Tian Y, Li N, Liu Y, Zhang J, Zhang J, Zuo W (2018) Highly-effective phosphate removal from aqueous solutions by calcined nano-porous palygorskite matrix with embedded lanthanum hydroxide. Appl Clay Sci 162:507–517

Kong M, Liu F, Tao Y, Wang P, Wang C, Zhang Y (2020) First attempt for in situ capping with lanthanum modified bentonite (LMB) on the immobilization and transformation of organic phosphorus at the sediment-water interface. Sci Total Environ 741:140342

Kong XJ, He T, Zhou J, Zhao C, Li TC, Wu XQ, Wang KC, Li JR (2021) In situ porphyrin substitution in a Zr (IV)-MOF for stability enhancement and photocatalytic $CO_2$ Reduction. Small 17(22):2005357

Lin JW, He S, Zhan Y, Zhang Z, Wu X, Yu Y, Zhao Y, Wang Y (2019) Assessment of sediment capping with zirconium-modified bentonite to intercept phosphorus release from sediments. Environ Sci Pollut Res 26:3501–3516

Lin JW, Zhao YY, Zhan YH, Wang Y (2020) Control of internal phosphorus release from sediments using magnetic lanthanum/iron-modified bentonite as active capping material. Environ Pollut 264:114809

Liu XL, Verma G, Chen ZS, Hu BW, Huang QF, Yang H, Ma SQ, Wang XK (2022) Metal-organic framework nanocrystals derived hollow porous materials: synthetic strategies and emerging applications. The Innovation 3(5):100281

Manciu FS, Reza L, Polette LA, Torres B, Chianelli RR (2007) Raman and infrared studies of synthetic Maya pigments as a function of heating time and dye concentration. J Raman Spec 38(9):1193–1198

McKeown DA, Post JE, Etz ES (2002) Vibrational analysis of palygorskite and sepiolite. Clay Clay Miner 50(5):667–680

Nguyen TT, Miyauchi M, Rahmatika AM, Cao KLA, Tanabe E, Ogi T (2022) Enhanced protein adsorption capacity of macroporous pectin particles with high specific surface area and an interconnected pore network. ACS Appl Mater Inter 14(12):14435–14446

Nkinahamira F, Alsbaiee A, Zeng Q, Li Y, Zhang Y, Feng M, Yu CP, Sun Q (2020) Selective and fast recovery of rare earth elements from industrial wastewater by porous beta-cyclodextrin and magnetic beta-cyclodextrin polymers. Water Res 181:115857

Ohashi Y, Wada T, Kato H (2022) High-entropy design and its influence on glass-forming ability in Zr–Cu-based metallic glass. J Alloys Compd 915:165366

Pan JM, Zou XH, Wang X, Guan W, Yan YS, Han J (2010) Selective recognition of 2,4-dichlorophenol from aqueous solution by uniformly sized molecularly imprinted microspheres with β-cyclodextrin/attapulgite composites as support. Chem Eng J 162:910–918

Qiu MQ, Liu LJ, Ling Q, Cai YW, Yu SJ, Wang SQ, Fu D, Hu BW, Wang XK (2022) Biochar for the removal of contaminants from soil and water: a review. Biochar 4(1):1–25

Rashid R, Shafiq I, Akhter P, Iqbal MJ, Hussain M (2021) A state-of-the-art review on wastewater treatment techniques: the effectiveness of adsorption method. Environ Sci Pollut R 28(8):9050–9066

Reitzel K, Lotter S, Dubke M, Egemose S, Jensen HS, Andersen FO (2013) Effects of Phoslock® treatment and chironomids on the exchange of nutrients between sediment and water. Hydrobiologia 703:189–202

Song Q, Huang S, Xu L, Wang N, Hu Z, Luo X, Zheng Z (2020) Synthesis of magnetite/lanthanum hydroxide composite and magnetite/aluminum hydroxide composite for removal of phosphate. Sci Total Environ 723:137838

Spears BM, Meis S, Anderson A, Kellou M (2013) Comparison of phosphorus (P) removal properties of materials proposed for the control of sediment P release in UK lakes. Sci Total Environ 442:103–110

Sun HM, Cao LY, Lu LH (2011) Magnetite/reduced graphene oxide nanocomposites: one step solvothermal synthesis and use as a novel platform for removal of dye pollutants. Nano Res 4(6):550–562

Wei WG, Shang N, Zhang X, Liu W, Zhang T, Wu M (2022) A green 3-step combined modification for the preparation of biomass sorbent from waste chestnut thorns shell to efficient removal of methylene blue. Bioresource Technol 360:127593

Xu R, Zhang M, Mortimer RJ, Pan G (2017) Enhanced phosphorus locking by novel lanthanum/aluminum–hydroxide composite: implications for eutrophication control. Environ Sci Technol 51:3418–3425

Yang WC, Li CF, Tian SQ, Liu LL, Liao Q (2020) Influence of synthesis variables of a sol-gel process on the properties of mesoporous alumina and their fluoride adsorption. Mater Chem Phys 242:122499

Yao L, Hu YZ, Zou YT, Ji ZY, Hu SX, Wang C, Zhang P, Yang H, ShenTangZhangZhaoWang ZwDYSGXXK (2022) Selective and efficient photoextraction of aqueous Cr (VI) as a solid-state polyhydroxy Cr (V) complex for environmental remediation and resource recovery. Environ Sci Technol 56:14030–14037

Ye H, Chen F, Sheng Y, Sheng G, Fu J (2006) Adsorption of phosphate from aqueous solution onto modified palygorskites. Separ Purif Technol 50:283–290

Yin H, Yan X, Gu X (2017) Evaluation of thermally-modifified calcium-rich attapulgite as a low-cost substrate for rapid phosphorus removal in constructed wetlands. Water Res 115:329–338

Yin HB, Yang P, Kong M, Li W (2020) Use of lanthanum/aluminum co-modified granulated attapulgite clay as a novel phosphorus (P) sorbent to immobilize P and stabilize surface sediment in shallow eutrophic lakes. Chem Eng J 385:123395

Yin HB, Zhang M, Huo L, Yang P (2022) Efficient removal of phosphorus from constructed wetlands using solidified lanthanum/aluminum amended attapulgite/biochar composite as a novel phosphorus filter. Sci Total Environ 833:155233

Yu SJ, Tang H, Zhang D, Wang SQ, Qiu MQ, Song G, Fu D, Hu BW, Wang XK (2021) MXenes as emerging nanomaterials in water purification and environmental remediation. Sci Total Environ 811:152280

Zhang Y, Pan B, Shan C, Gao X (2016) Enhanced phosphate removal by nanosized hydrated La(III) oxide confined in cross-linked polystyrene networks. Environ Sci Technol 50:1447–1454

Zhang YZ, Qin JF, Wang XJ, Chen ZG, Zheng XW, Chen YX (2021) Advanced treatment of phosphorus-containing tail water by Fe–Mg–Zr layered double hydroxide beads: performance and mechanism. J Environ Manage 296:113203

Zhou XY, Lu HY, Zhao F, Yu GH (2020) Atmospheric water harvesting: a review of material and structural designs. ACS Mater Lett 2(7):671–684

Zhu YS, Qiu S, Tang WW, Deng FX, Ma F, Zheng YS, Xie HJ (2022) Sustainable $Fe^{3+}$ reduction by $Fe_3O_4$@ tourmaline in Fenton-like system. Chem Eng J 437:135480